Contribution of Short-Range Intramolecular Interactions to Local Chain Dynamics

Canan Baysal, Burak Erman, and İvet Bahar*

Polymer Research Center, School of Engineering, Bogazici University, and TUBITAK Advanced Polymeric Materials Research Center, Bebek 80815, Istanbul, Turkey

Received October 21, 1993; Revised Manuscript Received April 7, 1994®

ABSTRACT: The effect of short-range intramolecular interactions on the probability distribution of conformational transitions between rotamers in polymers are examined by both numerical (Brownian dynamics simulations) and analytical (dynamic rotational isomeric state) methods. Simulations show, in agreement with analytical results, that the time-dependent conditional probability distributions of pair rotations are strongly affected by the interdependence of bond torsions. The latter are mainly induced by second order interactions, i.e. those occurring between pairs of atoms separated by four bonds. Comparison of numerical and analytical results demonstrates that the dynamic rotational isomeric state theory satisfactorily reproduces the stochastics of local conformational transitions observed in simulations. The average number of rotameric jumps occurring during a given time interval increases due to the interdependence of bond torsional states in polyethylene-like chains. This feature is manifested by an increase in the number of coupled transitions, favoring in particular gauche pair annihilations and correlated transitions among third neighboring bonds along the chain.

1. Introduction

Short-range intramolecular interactions in polymers have been broadly classified as first and second order interactions.[1] The former involves interactions between atoms separated by three bonds. The latter refers to those between atoms separated by four bonds. Chains composed of conformationally independent bonds are devoid of second order interactions.

The effect of second order interactions on equilibrium chain conformations in polymers has been addressed in numerous studies. In particular, the strong repulsive interactions between backbone atoms separated by four bonds when the middle two bonds assume *gauche* rotational states of opposite sign have been recognized to significantly effect the equilibrium statistics of polyethylene-like chains and are commonly referred to as the pentane effect. In the present study, the effects of such second order interactions on the *dynamics* of polymer chains are investigated. Two approaches are undertaken to assess the influence of bond interdependence on the mechanism of local motions: Brownian dynamics (BD) simulations and dynamic rotational isomeric state (DRIS) calculations. The latter is based on a master equation formalism and is the dynamic analogue of the rotational isomeric state theory[1] of polymer equilibrium statistics. It is an efficient method for studying local dynamics of chains of a given detailed chemical structure up to several nanoseconds.[2,3] Comparison of DRIS predictions with simulations will allow us to establish the validity and/or limitations of the DRIS formalism, in so far as the local conformational transitions of real chains are concerned.

In the original BD studies of polymers, simple models of bistable oscillators[4] and linked rigid bodies[5] have been used. More realistic model chains involving 3-fold symmetric rotation barriers have then been adopted to study stress, dielectric, mode, and conformational relaxation of chains.[6,7] The potential describing the rotational barriers has been modified from a cubic to a quintic,[8] by which the kinetics of conformational transitions in polyethylene-like chains have been investigated.[9,10] In those studies, backbone bonds were assumed to be subject to independent rotational potentials; i.e. no intrachain interactions other than chain connectivity and first order interactions along the chain were included. Cooperativity between torsional transitions of bonds i and $i + 2$ emerged in these studies as a requirement for the localization of the motion along the chain, thus stipulating the intrinsic effect of chain connectivity and geometry. The role of intrachain cooperativity in conformational transitions has been addressed by Adolf and Ediger in the BD study of polyisoprene.[11,12] A recent review by Adolf and Ediger gives a comprehensive summary of the work done using the BD method.[13] In the present work, the specific changes in the conformational dynamics of polyethylene-like chains arising from the inclusion of second order interactions are analyzed. To our knowledge, the present paper is the first BD study concentrating on the effect of rotational interdependence of first neighboring bonds and providing a precise comparison of the predictions of the DRIS approach with simulations.

The paper is organized so as (i) to compare simulations including second order interactions to those that do not and (ii) to provide a possible assessment of the validity of the DRIS formalism as a first approximation for treating local chain dynamics. Furthermore, the contribution of neighboring bond interdependence to the type and frequency of correlated transitions of longer range along the chain is analyzed. In section 2, the simulation method and parameters are described, and the DRIS formalism is reviewed briefly. In section 3, the results from simulations and DRIS calculations are presented. In part 3.A, probability distributions of bond rotational states, for either independent or interdependent pairs of bonds, are displayed. In part 3.B, transition probabilities for various pairs of rotameric states are presented and compared to those calculated by the DRIS scheme. In part 3.C, the cooperative transitions of pairs of bonds extending beyond first neighbors are examined. The most important rotational transition processes achieved in order to relax the chain locally are probed in part 3.D. Finally, in section 4, the conclusions of the study are summarized.

® Abstract published in *Advance ACS Abstracts*, May 15, 1994.

0024-9297/94/2227-3650$04.50/0

2. Theoretical Background

A. Brownian Dynamics Simulation with Interdependent Bond Potentials. A chain of $n+1$ backbone units, indexed from 0 to n, is considered. The notation of Flory[1] is adopted for designating bonds, bond angles, and torsional angles. The position vector of the ith backbone atom relative to the laboratory-fixed system is given by

$$\mathbf{r}_i = x_i\mathbf{e}_1 + y_i\mathbf{e}_2 + z_i\mathbf{e}_3 \qquad 0 \le i \le n \tag{1}$$

where x_i, y_i, z_i are the components of $\mathbf{r}$ along the respective base vectors $\mathbf{e}_1$, $\mathbf{e}_2$, and $\mathbf{e}_3$ of the coordinate system.

Each atom obeys the equation of motion:

$$\frac{d\mathbf{r}_i}{dt} = -\frac{1}{\zeta}\nabla_{\mathbf{r}_i}V + \mathbf{A}_i(t) \qquad 0 \le i \le n \tag{2}$$

where ζ is the friction coefficient, V is the total potential, $\nabla_{\mathbf{r}_i}$ denotes the gradient with respect to $\mathbf{r}_i$, and $\mathbf{A}_i(t)$ is a Gaussianly distributed random force with mean zero and covariance characterized by the correlation

$$\langle \mathbf{A}_i(t)\cdot\mathbf{A}_j(t')\rangle = \frac{2k_BT}{\zeta}\delta_{ij}\delta(t-t') \tag{3}$$

Here, k_B is the Boltzmann constant, T is the absolute temperature, δ_{ij} is the Kronecker delta, and $\delta(t-t')$ is the Dirac delta function. The gradient with respect to $\mathbf{r}_i$ in eq 2 represents the total force acting on the ith atom. The potential V is written as the sum

$$V = \sum_1^n V_l(l_i) + \sum_1^{n-1} V_\theta(\theta_i) + \sum_2^{n-1} V_\varphi(\varphi_i) + \sum_0^n V_{LJ}(\mathbf{r}_{ij}) \tag{4}$$

Here, $V_l(l_i)$ is the potential energy due to the stretching of ith bond, given by the harmonic function

$$V_l(l_i) = \frac{1}{2}k_l(l_i - l_{i0})^2 \tag{5}$$

where k_l is the bond stretching force constant, l_i is the instantaneous length of the bond between atoms $i-1$ and i, and l_{i0} is the equilibrium value about which the bond length fluctuates. The bond bending potential $V_\theta(\theta_i)$ is formulated by a similar expression,

$$V_\theta(\theta_i) = \frac{1}{2}k_\theta(\cos\theta_i - \cos\theta_{i0})^2 \tag{6}$$

with k_θ being the bending force constant, θ_i the instantaneous supplementary bond angle of the ith atom, and θ_{i0} its equilibrium value. Several types of torsional potential functions have been used in the literature, which are cubic or quintic functions of the dihedral angle. In the present simulations, the torsional potential, $V_\varphi(\varphi_i)$, proposed by Ryckaert et al.[8] and given by

$$V_\varphi(\varphi_i) = k_\varphi\sum_0^n a_n\cos^n\varphi_i \tag{7}$$

is used. Here k_φ is the torsional constant, φ_i is the torsional angle of the ith bond and the parameters a_n satisfy the proper distribution of the torsional potential. Equation 7 contains the sum of two effects: the intrinsic torsional potential and first order interactions between chain atoms. The intrinsic torsional potential is due to the sp^3 hybrids of tetrahedrally bonded atom groups. It leads to three equally probable minima at $\varphi = 0°, \pm120°$. The first order interactions induce a preference for the *trans* state ($\varphi = 0°$) relative to the *gauche* ($\varphi = \pm120°$) states, which is expressed by eq 7. Most BD simulations include only the potentials given by eqs 5–7.[5,9,14–17] An exception is the unsaturated hydrocarbon study of Rey et al.[18] The chain model with independent bonds using only V_l, V_θ, and V_φ (eqs 5–7) will be referred to as model I.

Second order interactions and long-range interactions including the excluded volume effect may be readily accounted for via the Lennard–Jones (LJ) 6–12 potential, $V_{LJ}(r_{ij})$

$$V_{LJ}(r_{ij}) = 4\epsilon_{ij}\left[\left(\frac{\sigma_{ij}}{r_{ij}}\right)^{12} - \left(\frac{\sigma_{ij}}{r_{ij}}\right)^{6}\right] \tag{8}$$

where $r_{ij} = |\mathbf{r}_j - \mathbf{r}_i|$, ϵ, and σ are the energy and length parameters characteristic of the specific pair of nonbonded atoms i and j, separated by four or more bonds. Interactions between atom pairs of index $|j-i| = 3$ are not included in eq 8, since those are accounted for by eq 7. In the present work, $V_{LJ}(r_{ij})$ will be taken as zero for $|j-i| \ge 5$. Thus, interactions between atoms that are close in their location in space but far from each other along the contour of the polymer are not considered in the calculations. Interactions with $|j-i| = 4$ leading to the pentane effect, on the other hand, are included. The chain model with such interdependent bonds in which the LJ potential (eq 8) is operative, in addition to the potentials given by eqs 5–7, will be referred to as model II.

The internal coordinates of the chain are described by the set of generalized coordinates $\{l_i, \theta_i, \varphi_i\}$. They are described in terms of the coordinates of atoms as

$$l_i = |\mathbf{r}_i - \mathbf{r}_{i-1}| \qquad 1 \le i \le n \tag{9}$$

$$\cos\theta_i = \frac{\mathbf{l}_i\cdot\mathbf{l}_{i+1}}{l_i l_{i+1}} \qquad 1 \le i \le n-1 \tag{10}$$

$$\cos\varphi_i = -\frac{\mathbf{l}_{i-1}\times\mathbf{l}_i}{|\mathbf{l}_{i-1}\times\mathbf{l}_i|}\frac{\mathbf{l}_i\times\mathbf{l}_{i+1}}{|\mathbf{l}_i\times\mathbf{l}_{i+1}|} \qquad 2 \le i \le n-1 \tag{11}$$

The gradients in eq 2 are obtained by using eqs 5–11, as given in detail elsewhere.[15]

The simulations are carried out for polyethylene chains of $n + 1 = 50$ units at 300 K. The temperature is maintained during the simulations through the random noise whose covariance obeys a temperature-dependent Gaussian distribution, according to eq 3. Thus, a fixed temperature is a consequence of the application of white noise, which acts as a constant temperature heat bath. No further temperature control is implemented in the simulation algorithm. The hydrogen atoms are assumed to be collapsed on the backbone atoms, and Lennard–Jones (LJ) parameters are chosen accordingly. There is a number of different values proposed for the LJ parameters ϵ and σ in literature.[10,12,18–20] Those of Sundararajan and Flory[19] are used here. The rest of the simulation parameters are the same as those in refs 10 and 15. The force constants for bending and bond stretching proposed by Helfand et al.[10] provide a reasonable compromise between realistic estimates leading to too fast oscillations and softer potentials allowing for larger time steps of integration.

A first configuration of the chain is generated by the Monte Carlo method using equilibrium values of bond lengths and bond angles. For the calculations with model II, the occurrence of $g^\pm g^\mp$ states in the original conformer is excluded, to avoid a highly unfavorable energy state in the original conformer. The integration time step is chosen

as 5×10^{-6} ns, which gives satisfactory convergence to equilibrium values. Equilibration runs of 10^5 time steps (0.5-ns total duration) are made in order to achieve more realistic orientations in space to be used at zero time. Results are recorded every 1000 steps until a 25-ns trajectory is performed. Calculations in section 3, parts C and D, require investigating very short time dynamics for which simulations with 5×10^{-7} ns time steps are performed for a total duration of 50 ns in the form of six independent trajectories, with results recorded every 200 steps.

B. DRIS Model. The DRIS model developed for investigating local chain dynamics has been applied to segments of polymer chains like polyethylene,[2] poly(ethylene oxide),[21] poly(dialkylsiloxanes),[22] and poly(isoprene).[23] The model is based on the master equation

$$d\mathbf{P}(t)/dt = \mathbf{A}\mathbf{P}(t) \tag{12}$$

where $\mathbf{P}(t)$ is the vector of time-dependent probabilities of all possible configurations and $\mathbf{A}$ is the transition rate matrix of the rate constants for the passage between configurations. Sequences of bond torsional states characterize a given configuration. Bond angles and lengths are assumed to be fixed at their equilibrium values. In general, the dynamic behavior of a given segment of n bonds with ν rotational isomeric states accessible to each bond is characterized by the set of eigenvalues λ_j of $\mathbf{A}$, with $j = 1$ to ν^N. For stationary processes, the elements of $\mathbf{P}(t)$ are independent of time and equal to the equilibrium probabilities of the ν^N configurations.

Precise determination of $\mathbf{A}$ is critically important for a realistic estimation of the conformational dynamics of polymers. In the simplest case of bonds subject to independent conformational energetics $\mathbf{A}$ is readily evaluated from the direct product of the transition rate matrices for independent bonds, and closed form expressions for the frequencies and distributions of isomerization modes are obtainable.[24] However, in most cases, consideration of the interdependence of neighboring bond rotational states is a basic requirement for establishing the connection between theory and experiments. Interdependence of bonds may be extended beyond first neighbors by considering simultaneous and/or coupled transitions of groups of bonds of size $n > 2$. Previous DRIS study of polyisoprene is an example in which coupled rotational dynamics of groups of three or more bonds were considered for the interpretation of dielectric relaxation behavior.[23] Inasmuch as the purpose of the present work is to understand the contribution of second order interactions to local conformational dynamics, we will confine our attention to the stochastics of pairwise interdependent bonds.

The types and activation energies of passages between pairs of rotameric states are found from conformational energy maps constructed as a function of adjacent torsional angles. For the case of bond pairs with $\nu = 3$ rotational states accessible to each bond, the operating transition rate matrix, denoted as $\mathbf{A}^{(2)}$, is given by a 9×9 matrix. The superscript in $\mathbf{A}^{(2)}$ refers to the number of interdependent bonds. The explicit form of $\mathbf{A}^{(2)}$ for bonds in polyethylene is given in the Appendix. In general, the off-diagonal element $\mathbf{A}^{(2)}_{ij}$ of $\mathbf{A}^{(2)}$ is the rate constant, k_{ij}, of passage from the jth isomeric state $\zeta\eta$ of the bond pair to the ith state $\zeta'\eta'$. k_{ij} is given by the Arrhenius-type expression $k_{ij} = A_0 \exp\{-E_{a,ij}/RT\}$ where R is the gas constant, T is the absolute temperature, and $E_{a,ij}$ is the activation energy for the particular transition $\zeta\eta \rightarrow \zeta'\eta'$. A_0 is the front factor related to the mobility of the system, which may be constructed to include the frictional resistance of the environment depending on the specific transition.

Table 1. Probabilities of Various States[a]

state	probability (model I)	probability (model II)
t	0.669	0.738
tt	0.445	0.512
$tg^{\pm}$ or $g^{\pm}t$	0.113	0.111
$g^{\pm}g^{\pm}$ or $g^{\mp}g^{\mp}$	0.026	0.018
$g^{\pm}g^{\mp}$ or $g^{\mp}g^{\pm}$	0.026	0.0014

[a] $g^{\pm}$ means g^+ and g^- states may be used interchangeably.

The master equation (12) is solved by using the transformation $\mathbf{A} = \mathbf{B}\Lambda\mathbf{B}^{-1}$ where Λ is the diagonal matrix of the eigenvalues of $\mathbf{A}$, $\mathbf{B}$ is the matrix of the eigenvectors of $\mathbf{A}$, and $\mathbf{B}^{-1}$ is the inverse of $\mathbf{B}$. The solution is written as

$$\mathbf{P}(t) = \mathbf{C}(t)\mathbf{P}(t = 0) = \mathbf{B}e^{\Lambda t}\mathbf{B}^{-1}\mathbf{P}(t = 0) \tag{13}$$

where $\mathbf{P}(t = 0)$ is the vector of the original probabilities of all configurations, $\mathbf{C}(t)$ is the time-dependent conditional probability defined by the second equality in eq 13. The ijth element $C(\zeta'\eta',t|\zeta\eta,0)$ of $\mathbf{C}(t)$ represents the time-delayed conditional probability of occurrence of state $\zeta'\eta'$ at time t, provided that the given pair of bonds assumes the state $\zeta\eta$ at $t = 0$.

The transition probability $C(\zeta'\eta',t|\zeta\eta,0)$ may also be calculated by BD since, for a stationary process, as presently studied, the time origin is immaterial, but the time interval t between two successive states is important. Thus, data recorded at various time origins along the trajectory are suitably combined to evaluate $C(\zeta'\eta',t|\zeta\eta,0)$, provided that $t \ll t^*$, where t^* is the total duration of the simulation.

3. Calculations and Results

A. Probability Distributions of Bond Torsional Angles. First we consider the distribution of bond rotational angles resulting from simulations. The *trans* probabilities are obtained as 0.669 and 0.738, using models I and II, respectively (Table 1). These are evaluated from the average over all bonds i, excluding the five terminal bonds at both ends, i.e. $6 \leq i \leq n - 5$. Likewise, all equilibrium and transition probabilities reported below are determined from the average behavior of the same subset of internal bonds. Although the stretching, bending, and torsion parameters are the same in both models, the *trans* population is enhanced in model II. This is a direct consequence of the inclusion of second order interactions. The probability of *trans* conformers obtained for model II agrees with the molecular dynamics (MD) value of 0.718 calculated by Rigby and Roe[12] for 20-segment chains at 301 K.

The equilibrium probability distributions $p(\varphi_i,\varphi_{i+1})$ for the joint state of two consecutive dihedral angles, φ_i and φ_{i+1}, exhibit the difference between models I and II clearly. The cross-section at $-120°$ of the two-dimensional probability distribution surface resulting from models I and II is displayed in Figure 1. The peaks belonging to g^+g^- and g^-g^- are identical therein for model I. In the curve for model II, however, the peak belonging to g^+g^- is absent altogether. The energy difference between these two distinct states, E_ω, may be estimated from

$$E_\omega = -RT \ln\left[\frac{p_{g^+g^-}}{p_{g^+g^+}}\right] \tag{14}$$

where $(p_{g^+g^-}/p_{g^+g^+})$ is the ratio of the equilibrium prob-

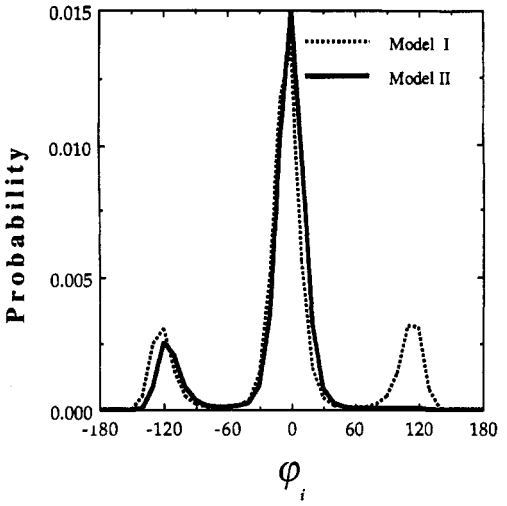

Figure 1. Probability distribution of bond dihedral angles φ_i, given the state $\varphi_{i+1} = -120°$. The dashed and solid curves are obtained for chains with independent and pairwise interdependent bonds, respectively. The peak at the g^+g^- state (+120°, −120°) disappears as expected.

abilities $p_{g^+g^-}$ and $p_{g^+g^+}$ of the respective rotameric states $g^\pm g^\mp$ and $g^\pm g^\pm$ for consecutive bonds. The probability of a state is evaluated from the volume element enclosed under the corresponding peak in the normalized probability distribution surface.[22,25,26] For example, $p_{g^+g^-}$ is evaluated from

$$p_{g^+g^-} = \frac{\int_{-\pi}^{-\pi/3}\int_{\pi/3}^{\pi} P(\varphi_i,\varphi_{i+1})\, d\varphi_i\, d\varphi_{i+1}}{\int_{-\pi}^{\pi}\int_{-\pi}^{\pi} P(\varphi_i,\varphi_{i+1})\, d\varphi_i\, d\varphi_{i+1}} \qquad (15)$$

the integration therein being approximated by summation over grids of size 10°. The probabilities of various states calculated accordingly by adding up discrete probabilities at the center of surface elements of 10° × 10° intervals are presented in Table 1. In model I, there is no difference between the probabilities of $g^\pm g^\mp$ and $g^\pm g^\pm$ states, and hence $E_\omega = 0$. In model II, on the other hand, an E_ω value of 1.54 kcal/mol is obtained by using eqs 14 and 15. A more rigorous relationship which makes use of interdependent probability distribution surfaces of the MD trajectories for the formulation of statistical weight matrices is given by Mattice et al.[25] Using that scheme, E_ω turns out to be 1.47 kcal/mol. We note that in the original work of Abe, Jernigan, and Flory[27] a value of E_ω = 2.0 kcal/mol is adopted. The use of a lower E_ω has the effect of reducing the characteristic ratio of polyethylene, although this effect may be more than counterbalanced by varying the equilibrium dihedral angle $\varphi_{g^\pm}$ of the $g^\pm$ state. Ranges of parameter E_ω affording good agreement with experiments on the characteristic ratio and its temperature coefficient are pointed out[1] to be $1.7 \le E_\omega \le 2.0$ kcal/mol for $\varphi_{g^\pm} = \pm 120°$ and $1.3 \le E_\omega \le 1.6$ kcal/mol for $\varphi_{g^\pm} = \pm 112.5°$, which are in satisfactory agreement with the value $E_\omega = 1.51 \pm 0.04$ presently obtained.

B. Conditional Probabilities of Rotational Transitions. (i) Comparison of BD Results from Models I and II. Time-dependent conditional probabilities of bond rotations give information both on the dynamics of transitions between isomeric states and on their equilibrium probabilities. The conditional probabilities, $C(\zeta'\eta',t|\zeta\eta,0)$, are obtained by tabulating the total number of initial and final states assumed by two consecutive bonds at various time differences t and then dividing these by the sum of the 81 different transitions recorded. Table 2 gives a list of the most probable transitions of pairs of adjacent bonds, $\zeta\eta \rightarrow \zeta'\eta'$. Here ζ and η stand for the rotational isomeric states, t, g^+, and g^-. In the transitions 1–4, the original pair of rotameric states $\zeta\eta$ is identical to the final state $\zeta'\eta'$. Thus, in a strict sense, those are not passages between rotameric states but refer to the cases in which the state of a given bond pair remains unchanged.

Table 2. Most Probable Pairs of Initial and Final States[a]

type of states	$\zeta\eta \rightarrow \zeta'\eta'$	type of states	$\zeta\eta \rightarrow \zeta'\eta'$
1	$tt \rightarrow tt$	7	$g^\pm g^\pm \rightarrow tg^\pm$
2	$tg^\pm \rightarrow tg^\pm$		$g^\pm g^\pm \rightarrow g^\pm t$
	$g^\pm t \rightarrow g^\pm t$	8	$g^\pm g^\mp \rightarrow tg^\mp$
3	$g^\pm g^\pm \rightarrow g^\pm g^\pm$		$g^\pm g^\mp \rightarrow g^\pm t$
4	$g^\pm g^\mp + g^\pm g^\mp$	9	$g^\pm g^\mp \rightarrow tt$
5	$g^\pm t \rightarrow tt$	10	$g^\mp t \rightarrow tg^\pm$
	$tg^\pm \rightarrow tt$		$tg^\pm \rightarrow g^\mp t$
6	$tt \rightarrow tg^\pm$		
	$tt \rightarrow g^\pm t$		

[a] In cases 1–4 the states of the bonds remain unchanged; cases 5–10 refer to rotational transitions of one or both bonds of the pair.

First, we study the time evolution of $C(\zeta'\eta',t|\zeta\eta,0)$ in the absence of bond interdependence. The results for those cases with $\zeta'\eta' = \zeta\eta$ and $\zeta'\eta' \neq \zeta\eta$ are presented in Figure 2a,b, respectively. In these figures, the values asymptotically approached represent the equilibrium probabilities of the state $\zeta'\eta'$ and are consistent with the values in Table 1. It is also worth noting that in all the curves, equilibrium probabilities have been reached within 1 ns. The transitions $g^\pm g^\pm \rightarrow g^\pm g^\pm$ and $g^\pm g^\mp \rightarrow g^\pm g^\mp$ obey identical kinetics in the absence of secondary interactions; these are represented by the curve labeled 3,4 in Figure 2a. This follows from the equivalence of $g^\pm g^\pm$ and $g^\pm g^\mp$ states when bond interdependence is neglected. The same is true for transitions $g^\pm g^\pm \rightarrow g^\pm t$ and $g^\pm g^\mp \rightarrow g^\pm t$ (curve 7,8 in Figure 2b).

The counterpart of Figure 2a in the presence of second order interactions is Figure 3a. That of Figure 2b is presented in two distinct figures, 3b and 3c, for clarity. The major difference between results from models I and II is observed in the time evolution of the pair of *gauche* bonds. In model II, the passage $g^\pm g^\mp \rightarrow g^\pm g^\mp$ (curve 4 in Figure 3a) is distinct from $g^\pm g^\pm \rightarrow g^\pm g^\pm$ (curve 3 in Figure 3a), there is an immediate escape from the state $g^\pm g^\mp$, and the corresponding low equilibrium value is quickly reached. One can also observe that the transition probabilities for the passages $g^\pm g^\pm \rightarrow g^\pm t$ and $g^\pm g^\mp \rightarrow g^\pm t$ (i.e. curve 7 in Figure 3b and curve 8 in Figure 3c) reach a maximum at short times, before converging to the equilibrium probability of the $g^\pm t$ state. In particular, that of $g^\pm g^\mp \rightarrow g^\pm t$ is very pronounced, in contrast to the time dependence of the same transition displayed (Figure 2b) in the absence of second order interactions along the chain.

In the transition curves for model II, the fluctuations in the time evolution of the passage $g^\pm g^\mp \rightarrow tt$ and $g^\pm g^\mp \rightarrow tg^\pm$ (curves 9 and 8 in Figure 3c) are due to the very small sample space of the $g^\pm g^\mp$ population. The $g^\pm g^\mp \rightarrow tg^\pm$ transition is affected by the strong tendency to escape from the $g^\pm g^\mp$ state, indicated by the short time peak in the 30-ps range in Figure 3c. It has a time dependence separate from that of the $g^\pm g^\pm \rightarrow tg^\pm$ transition, whereas the two transitions are represented by the same curve for model I (Figure 2b).

The two transitions $g^\pm t \rightarrow tt$ (curve 5, Figure 3b) and $g^\pm g^\mp \rightarrow tt$ (curve 9, Figure 3c) exhibit similar time dependences in model II provided that the oscillations induced by the $g^\pm g^\mp$ state are overlooked. This phenomena is explained by the two-step character of transition 9, which occurs through the mechanism $g^\pm g^\mp \rightarrow tg^\pm \rightarrow tt$. Here,

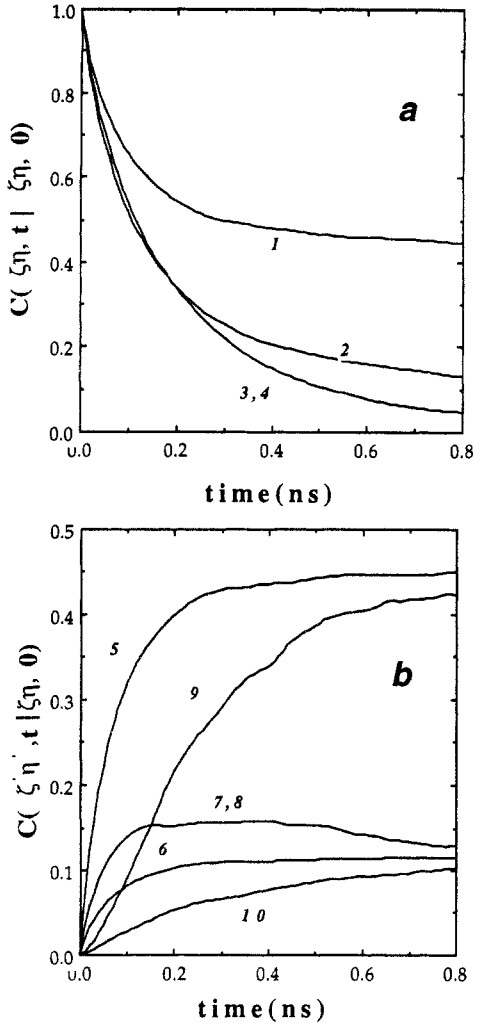

Figure 2. (a) Time-dependent conditional probabilities $C(\zeta\eta,t|\zeta\eta,0)$ for maintaining the state $\zeta\eta$ of bond pairs subject to independent rotational potentials. (b) Time-dependent conditional probabilities $C(\zeta'\eta',t|\zeta\eta,0)$ for bond pairs subject to independent rotational potentials; the final state of the bonds changes such that one or both of the bonds undergo a transition ($\zeta'\eta' \neq \zeta\eta$). Labels on the curves correspond to transitions identified in Table 2.

the first transition (curve 8, Figure 3c) is fast, and the second, which corresponds to transition 5 itself, is the rate controlling one. The same argument cannot be made for model I, since the two steps of transition 9 evolve in comparable times. As a result, there are two distinct curves corresponding to transitions 5 and 9, as shown in Figure 2b.

From the above comparison, we deduce that the types and rates of rotational transitions taking place during the Brownian motion of real chains are rather sensitive to second order interactions along the chain. The second order interactions result in the coupling of the torsional states and transitions of neighboring bonds and give rise to a mechanism of relaxation different from that observed in the absence of bond interdependence, as described above in terms of the time evolution of transition probabilities. Simulations with energy functions and parameters disregarding second order interactions along the chain, as has been performed in a number of BD studies, may lead to serious departure from real chain behavior and should be interpreted with caution.

(ii) Comparison of DRIS Results to BD Simulations with Model II. Results of DRIS calculations at 300 K are presented by the circles and triangles in Figure 3a–c.

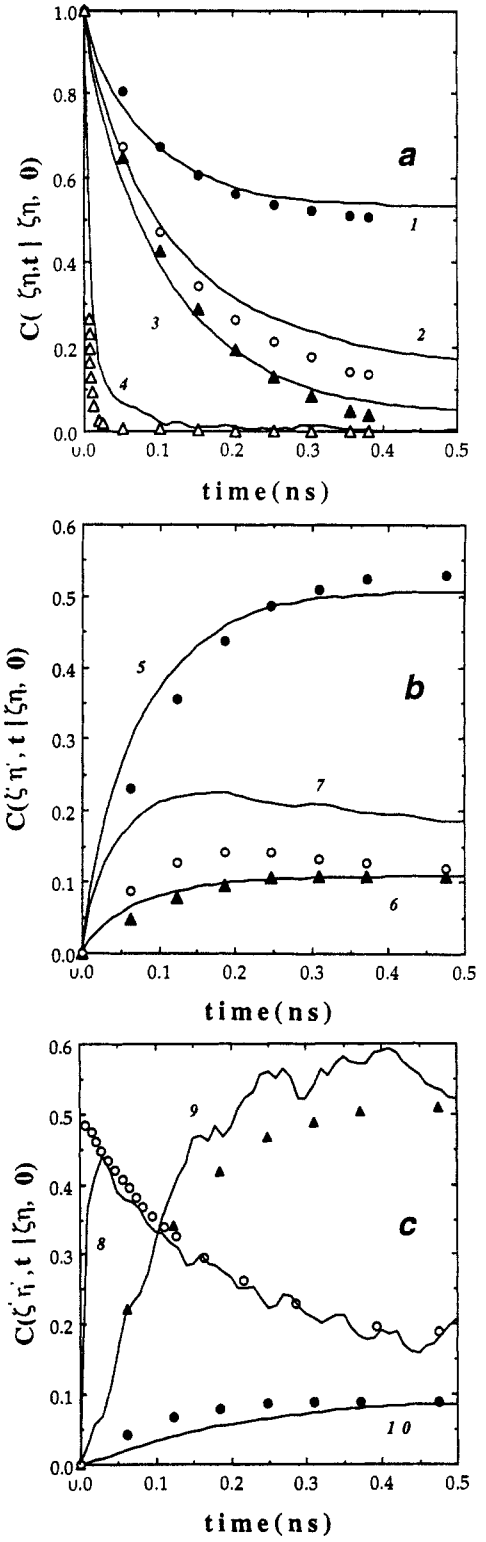

Figure 3. (a) Time-dependent conditional probabilities $C(\zeta'\eta',t|\zeta\eta,0)$ from BD simulations for bond pairs with interdependent rotational potentials ($\zeta'\eta' = \zeta\eta$). Labels on the curves correspond to transitions identified in Table 2. (b) Time-dependent conditional probabilities $C(\zeta'\eta',t|\zeta\eta,0)$ from BD simulations for bond pairs with interdependent rotational potentials for transitions identified as 5–7 in Table 2 and labeled on the curves. (c) Time-dependent conditional probabilities $C(\zeta'\eta',t|\zeta\eta,0)$ from BD simulations for bond pairs with interdependent rotational potentials for transitions identified as 8–10 in Table 2 and labeled on the curves. Circles and triangles represent DRIS results.

The calculations are performed with the kinetic scheme and activation energy data given in ref 2. The basic assumption therein is the pairwise interdependence of

bonds, and the reader is referred to the Appendix for the explicit form of the transition matrix $A^{(2)}$. In order to compare the results from the DRIS approach with those of BD in the presence of bond interdependence, the front factor A_0, which accounts for the frictional resistance to motion in the expressions for k_{ij}, is adjusted to match that of BD simulations ($\zeta = 10^5$ ns^{-1}). Hence, A_0 is rescaled to fit the $tt \rightarrow tt$ decay curve (1) of the two approaches, which yields $A_0 = 5.72 \times 10^{11}$ s^{-1}. When this value is used in the rest of the calculations for all transitions, not only qualitative but also quantitative, correspondence between the DRIS model and BD simulations has been accomplished.

In both techniques, equilibrium values are reached within 1 ns. DRIS predicts a slightly stronger tendency to escape from the $g^{\pm}g^{\mp}$ state compared to BD. This is attributed to the fact that part of the repulsive force produced in the $g^{\pm}g^{\mp}$ state is normally taken on by the distortions in the bond lengths and angles so that the escape from this configuration is weakened. However, these distortions are not included in the DRIS method. The only transition where there is no quantitative agreement is $g^{\pm}g^{\pm} \rightarrow tg^{\pm}$ (transition 7 in Figure 3b). There, the passage through a peak is well predicted by DRIS but the equilibrium value of 0.11 is reached quicker than it is with BD simulations. On the other hand, here BD simulations exhibit a faster rate of escape from the $g^{\pm}g^{\pm}$ state at short times. In all other curves there is good qualitative and quantitative agreement between the results from BD and those from DRIS. This proves DRIS to be a well suited method for the prediction of bond pair dynamics.

C. Near Neighbor Transitions. The importance of correlated transitions occurring among near neighbors along the chain has been pointed out in BD studies,[9-11] and later discussed in the MD simulations of Zuniga et al.[26] Successive transitions occurring within 5 ps, approximately, are identified as correlated transitions, in general. In the present study, first passage times between successive transitions have been accordingly analyzed in BD trajectories resulting from both models I and II. Simulations of six different starting configurations, using 10 times shorter time steps, i.e. 5×10^{-7} ns, have been followed up to a total duration of 50 ns. The regions determining the isomeric states have been identified as in ref 24 as $|\varphi_i| < 30°$ for t and $+90° < |\varphi_i| < 135°$ for $g^{\pm}$; the rest of the dihedral angles are assigned their last definite states. This procedure avoids the redundant counting of passages over saddle points, during the evaluation of first passage times between rotational isomeric states. A total of 12 310 transitions have been recorded using model I, whereas 13 981 transitions occur during the same time interval, with the same initial configurations, when model II is used. Thus, the presence of a high energy state ($g^{\pm}g^{\mp}$) renders the chains of model II more susceptible (by 14%) to rotational transitions.

The time evolution of coupled transitions between near neighbors from six different trajectories of total duration 50 ns is shown in Figure 4. The solid curves in the figure are calculated using model I, for the pair of second and third neighbors, as indicated by the labels; their counterparts obtained with model II are shown by the dashed curves. These curves are calculated according to the following procedure: First, the time at which a given bond k undergoes an isomeric jump is recorded; then, one observes the ith topological neighbor, and the time interval Δt elapsed until bond $k + i$ changes its rotational state is recorded. This procedure is repeated up to $\Delta t = 2$ ps, for all internal bonds in the chain, throughout the whole

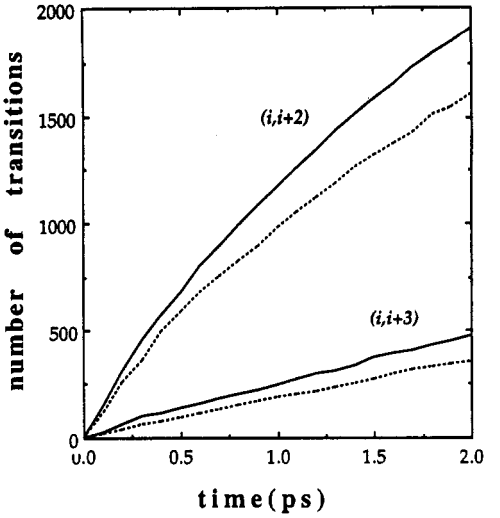

Figure 4. Time evolution of coupled transitions among second and third neighbors along the chain. The solid and dashed curves are obtained from BD simulations with models I and II, respectively, demonstrating that the number of coupled transitions between second and third neighbors, i.e. the pairs (i, i + 2) and (i, i + 3), respectively, is enhanced when second order interactions along the chain are incorporated in the model.

trajectory, except for the terminal five bonds, which are not considered because of end effects. The number of coupled transitions between second and third neighbors was found to increase by the interdependence of backbone torsional states, as may be observed from the deviations between the solid and dashed curves in Figure 4. In particular, we note that the number of coupled transitions between third neighbors ($i = \pm 3$) increases by 42%. Those between second neighbors ($i = \pm 2$) increase by 35%. The results for $i = 1$ and 4, whose frequencies of occurrence were lower compared to $i = 2$ or 3, are not displayed in the figure, for clarity. Those of first neighbors ($i = 1$) are also augmented (by ~30%) upon consideration of second order interaction, whereas the number of correlated transitions between fourth neighbors was almost insensitive to the model, suggesting that correlated transitions involving farther neighbors, if any, are less affected by second order interactions. Calculations performed for farther neighbors ($i = 10$, for instance) verified that the corresponding time evolution curves exhibit the same behavior as that of the overall ensemble of transitions (15% deviation), and hence the rotational motions of such distant bonds are not affected by intramolecular correlations.

D. Mechanisms for Localization of Motion. When a transition occurs at one of the internal bonds of a chain, the near neighbors of the rotating bond rearrange so as to minimize the spatial displacements of the atoms and the total energy of the system. If a rotational jump of a reference is accompanied by small rotations (±30°) of the nearby bonds, this is called an *isolated* transition. Alternatively, the polymer may compensate for the energy difference created by a rotational transition by making a *cooperative* rotameric transition at one or more neighboring bonds. Well-known mechanisms of the latter type are *gauche* migration ($g^{\pm}tt \leftrightarrow ttg^{\pm}$), *gauche* pair creation ($ttt \rightarrow g^{\pm}tg^{\mp}$), and *gauche* annihilation ($g^{\pm}tg^{\mp} \rightarrow ttt$).[28,29] These are identified as type II motions where the remainder of the chain does not change shape but just translates.

Of the total number of transitions taking place within the 50-ns trajectories of part C, the percentage of isolated transitions is found to be 70.3 ± 0.05% at 300 K, irrespective of second order interactions. We note that this proportion of isolated and cooperative transitions

Table 3. Number of Most Probable Cooperative Transitions among Second Neighbors

transition	model I	model II	% increase
$g^{\pm}tt \leftrightarrow ttg^{\pm}$	957	1144	20
$ttt \rightarrow g^{\pm}tg^{\mp}$	395	479	21
$g^{\pm}tg^{\mp} \rightarrow ttt$	338	430	27

compares favorably with that (70.7%) obtained at 330 K by Weber and Helfand[28] in the absence of second order interactions.

Although the proportion of the cooperative transitions among all transitions is the same in both models, the distributions among different types of passages are different in the two approaches. For example, the numbers of the most frequently occurring types of second neighbor transitions are presented in Table 3. The last column indicates the percent change in the rates of those passages upon inclusion of second order interactions. There is a considerable increase in these transitions, which is substantially larger than the overall enhancement of transition rates (i.e. 14%) in model II. In particular, *gauche* pair annihilation, shown in the third row of the table, is found to increase by 27% upon inclusion of second order interactions.

We note that in both models the frequency of *gauche* pair creation exceeds that of *gauche* pair annihilation. This might suggest at first sight some gradual increase and eventual saturation in the population of *gauche* states during simulations. However, it should be recalled that Table 3 is constructed for a subset of transitions only, mainly *cooperative* transitions among *second* neighbors. There is a much larger number of transitions, either isolated or cooperative between other neighbors, contributing to the equilibration of the population of different rotameric states and maintaining the state of dynamic equilibrium (detailed balance) conforming with the specific chain statistics.

IV. Conclusions

The major results of the present work are summarized as follows:

1. The mechanism of conformational relaxation is strongly affected by second neighbor interactions along the chain. Specifically, upon inclusion of second order interactions in the simulation model the time evolution of the transitions $g^{\pm}g^{\pm} \rightarrow g^{\pm}t$, $g^{\pm}g^{\mp} \rightarrow g^{\pm}t$, $g^{\pm}t \rightarrow tt$, and $g^{\pm}g^{\mp} \rightarrow tt$ changes drastically, as illustrated in the respective curves 7, 8, 5, and 9 of Figures 2b and 3b,c.

2. The comparison of BD results obtained in the presence of second order interactions, with the predictions of the analytical DRIS theory in Figure 3a–c shows that the DRIS formalism gives a satisfactory account of the probability distributions and rates of particular rotameric transitions. A major shortcoming of the DRIS formalism is that the tails are free to translate following a rotameric transition over an internal bond. In this sense, long-range chain connectivity is not rigorously taken into account in the DRIS formalism. The BD method, on the other hand, intrinsically incorporates cooperative interactions of longer-range resulting from chain connectivity. Despite this basic difference between the two methods, we observe in Figure 3a–c that passages between rotameric states of bond pairs obey similar time evolutions in the two approaches. This is an important observation which lends support to the use of the DRIS approach for describing the dynamics of local conformational motions in polymers.

3. The overall conformational mobility of the chain is enhanced upon inclusion of second order interactions. Thus, the number of rotameric jumps is increased by 14%. This increase is equally distributed among cooperative and isolated transitions. However, certain types of the cooperative transitions, such as *gauche* migration, *gauche* pair creation, and *gauche* pair annihilations exhibit an even stronger (by 20, 21, and 27%, respectively) enhancement. On the other hand, coupled transitions occurring within 2 ps among third neighbors undergo an increase of 42%, in the presence of second order interactions.

Appendix

The transition rate matrix for interdependent bond pairs for polyethylene reads

$$\mathbf{A}^{(2)} = \begin{bmatrix} A_{11} & r_{-1} & r_{-1} & r_{-1} & 0 & 0 & r_{-1} & 0 & 0 \\ r_1 & A_{22} & 0 & 0 & r_{-2} & 0 & 0 & r_{-3} & 0 \\ r_1 & 0 & A_{33} & 0 & 0 & r_{-3} & 0 & 0 & r_{-2} \\ r_1 & 0 & 0 & A_{44} & r_{-2} & r_{-3} & 0 & 0 & 0 \\ 0 & r_2 & 0 & r_2 & A_{55} & 0 & 0 & 0 & 0 \\ 0 & 0 & r_3 & r_3 & 0 & A_{66} & 0 & 0 & 0 \\ r_1 & 0 & 0 & 0 & 0 & 0 & A_{77} & r_{-3} & r_{-2} \\ 0 & r_3 & 0 & 0 & 0 & 0 & r_3 & A_{88} & 0 \\ 0 & 0 & r_2 & 0 & 0 & 0 & r_2 & 0 & A_{99} \end{bmatrix} \quad \text{(A-1)}$$

where the diagonal elements are evaluated from the negative sum of the remaining elements in the corresponding column and r_i ($i = \pm 1$ to ± 3) refer the rate constants of the transitions shown below:

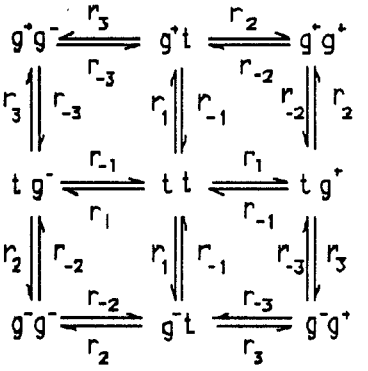

(A-2)

Acknowledgment. Partial support from Bogazici University Research Fund Project No. 94P0002 is gratefully acknowledged.

References and Notes

(1) Flory, P. J. *Statistical Mechanics of Chain Molecules*; Interscience: New York, 1969.
(2) Bahar, I.; Erman, B. *Macromolecules* **1987**, *20*, 1368.
(3) Bahar, I.; Erman, B.; Monnerie, L. *Adv. Polym. Sci.*, in press.
(4) Helfand, E. *J. Chem. Phys.* **1978**, *69*, 1010.
(5) Pear, M. R.; Weiner, J. *J. Chem. Phys.* **1979**, *71*, 212.
(6) Fixman, M. *J. Chem. Phys.* **1978**, *69*, 1527.
(7) Fixman, M. *J. Chem. Phys.* **1978**, *69*, 1538.
(8) Ryckaert, J. P.; Bellemans, A. *Chem. Phys. Lett.* **1975**, *30*, 123. Liang, G. L.; Noid, D. W.; Sumpter, B. G.; Wunderlich, B. *Comput. Polym. Sci.* **1993**, *3*, 101.
(9) Helfand, E.; Wasserman, Z. R.; Weber, T. A. *J. Chem. Phys.* **1979**, *70*, 2016.
(10) Helfand, E.; Wasserman, Z. R.; Weber, T. A. *Macromolecules* **1980**, *13*, 526.
(11) Adolf, D. B.; Ediger, M. D. *Macromolecules* **1991**, *24*, 5834.
(12) *Computer Simulation of Polymers*; Roe, R. J., Ed.; Prentice Hall: New York, 1990.
(13) Ediger, M. D.; Adolf, D. B. *Adv. Polym. Sci.*, in press.
(14) Pear, M. R.; Weiner, J. H. *J. Chem. Phys.* **1980**, *72*, 3939.
(15) Haliloglu, T.; Bahar, I.; Erman, B. *J. Chem. Phys.* **1992**, *97*, 4428.
(16) Haliloglu, T.; Bahar, I.; Erman, B. *J. Chem. Phys.* **1992**, *97*, 4438.
(17) Adolf, D. B.; Ediger, M. D. *Macromolecules* **1991**, *24*, 5834.

(18) Rey, A.; Kolinski, A.; Skolnick, J.; Levine, Y. K. *J. Chem. Phys.* **1992**, *97*, 1240.
(19) Sundararajan, P. R.; Flory, P. J. *J. Am. Chem. Soc.* **1974**, *96*, 1117.
(20) Rigby, D.; Roe, R.-J. *J. Chem. Phys.* **1987**, *78*, 7285.
(21) Bahar, I.; Erman, B.; Monnerie, L. *Macromolecules* **1989**, *22*, 2396.
(22) Bahar, I.; Neuburger, N.; Mattice, W. L. *Macromolecules* **1992**, *25*, 4620.
(23) Bahar, I.; Erman, B.; Kremer, F.; Fischer, E. W. *Macromolecules* **1992**, *25*, 816.
(24) Kloczkowski, A.; Mark, J. E.; Bahar, I.; Erman, B. *J. Chem. Phys.* **1990**, *92*, 4513.
(25) Mattice, W. L.; Dodge, R.; Zuniga, I.; Bahar, I. *Comput. Polym. Sci.* **1991**, *1*, 35.
(26) Zuniga, I.; Bahar, I.; Dodge, R.; Mattice, W. L. *J. Chem. Phys.* **1991**, *95*, 5348.
(27) Abe, A.; Jernigan, R. L.; Flory, P. J. *J. Am. Chem. Soc.* **1966**, *88*, 631.
(28) Weber, T. A.; Helfand, E. *J. Phys. Chem.* **1983**, *87*, 2881.
(29) Bahar, I.; Erman, B.; Monnerie, L. *Macromolecules* **1992**, *25*, 6315.